Chemical Engineering Journal 283 (2016) 1264–1272

Contents lists available at ScienceDirect

Chemical Engineering Journal

journal homepage: www.elsevier.com/locate/cej

TiO_2 thick films supported on stainless steel foams and their photoactivity in the nonylphenol ethoxylate mineralization

Salatiel Wohlmuth da Silva [a,b], Juan Pablo Bortolozzi [b], Ezequiel David Banús [b], Andréa Moura Bernardes [a], Maria Alicia Ulla [b,*]

[a] Universidade Federal do Rio Grande do Sul – UFRGS – (PPGE3M, Lacor), Av. Bento Gonçalves, 9500 Porto Alegre/RS, Brazil
[b] Instituto de Investigaciones en Catálisis y Petroquímica – INCAPE (FIQ, UNL – CONICET), 3000 Santa Fe, Argentina

HIGHLIGHTS

- TiO_2 powder was successfully immobilized via washcoating onto metallic foam walls.
- The TiO_2 film presented high adherence and was free of cations from the foam core.
- The crystalline composition of the TiO_2 powder remained on the TiO_2 layer so obtained.
- TiO_2-foam showed an interesting photocatalytic performance in the NP_4EO degradation.

GRAPHICAL ABSTRACT

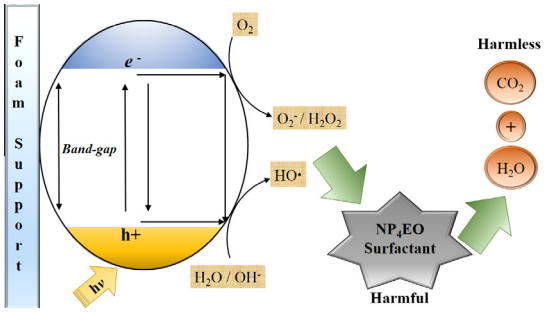

ARTICLE INFO

Article history:
Received 29 May 2015
Received in revised form 31 July 2015
Accepted 1 August 2015
Available online 28 August 2015

Keywords:
Titanium oxide
Heterogeneous photocatalysis
Emerging contaminant
Nonylphenol ethoxylate

ABSTRACT

The main interest in employing a structured catalyst for water treatment processes is to avoid an extra recovering-step of the powder catalyst after concluding the treatment. For this purpose, TiO_2 powder (Degussa P25) was immobilized onto metallic foam walls (TiO_2-foam) through the washcoating method and its photocatalytic activity was evaluated in the degradation of nonylphenol ethoxylate (NP_4EO), which is considered an endocrine disrupter. The morphological and physicochemical characteristics of TiO_2 films were studied by X-ray Diffraction, Laser Raman Spectroscopy and Scanning Electron Microscopy.

The fast and easy washcoating method used in this work allowed the immobilization of the TiO_2 powder onto a relatively inexpensive metallic substrate. The TiO_2 layer was uniformly distributed, having a high adherence to the metallic foam walls, which were previously submitted to a passivation treatment. This pre-treatment hindered a further migration of cations from the foam core to the titania film and favored the subsequent film anchorage. Moreover, the catalytic film so obtained maintained the anatase and rutile phases with their original proportions, preserving the properties of the TiO_2 powder. The photocatalytic activity of the TiO_2-foam was similar to that of a commercial catalyst (TiO_2–Ti mesh), i.e. both reduced the TOC of the NP_4EO solution by about 91%, showing similar reaction kinetics and overall quantum yield ($\Phi_{overall}$). These results demonstrate that by means of the method under study, TiO_2 can be successfully immobilized without decreasing its photocatalytic activity. These catalysts may be applied in water/wastewater treatment, reducing the process stages and the overall cost of the procedure.

* Corresponding author.
E-mail address: mulla@fiq.unl.edu.ar (M.A. Ulla).

http://dx.doi.org/10.1016/j.cej.2015.08.057
1385-8947/

1. Introduction

The overwhelming discharge of contaminants from the electroplating industry into natural water cycles makes it imperative to develop effective technologies for the purification of wastewater, prior to releasing it into natural channels. In this vein, the industrial wastewater treatment with biological processes is often ineffective because this kind of wastewaters is usually polluted with non-biodegradable organic compounds. Some Advanced Oxidation Processes (AOPs) can be applied in these cases. These processes require the addition of chemicals and a high level of energy to induce the formation of hydroxyl radicals ($HO^{\cdot}$), which are the active species for the degradation of recalcitrant molecules. Besides, heterogeneous photocatalysis and homogeneous photo-Fenton processes can also be used, both sharing the requirement of UV irradiation [1,2]. Among the techniques developed for the removal of emerging contaminants, heterogeneous photocatalysis has attracted considerable interest in recent years [3–8]. TiO_2 has been known as the leading photocatalyst among various semiconductors due to its high photo-activity and chemical stability, low cost, nontoxicity and resistance to photo-corrosion [9].

Several authors have reported the use of TiO_2 (Degussa P25) in the process of heterogeneous photocatalysis [5,6,8,10]. This commercial TiO_2 presents an excellent photocatalytic activity mainly due to its combined crystalline structure, 75% anatase and 25% rutile. This arrangement of anatase–rutile produces a synergetic performance inducing a slow recombination between electrons and holes [5,6], which has a positive effect on its photocatalytic properties. On the other hand, the mechanisms of photocatalysis are well known and have been discussed by Hoffmann et al. [9] and Mills et al. [11] in their respective reviews.

A semiconductor photocatalyst can be employed either in a colloidal form or as an immobilized film. According to several results reported in the literature, TiO_2 suspension is the best way to use this solid as a photocatalyst [12–15]. However, applying photoreactors operated with catalytic colloidal particles for water and wastewater treatment processes require an extra recovering-step after concluding the treatment, which means a costly and time-consuming process. This inconvenience could be avoided by immobilizing the catalyst onto a substrate bringing about many operational advantages. Even though an extra cost is added due to the catalyst immobilization procedure, it is possible to reduce the overall process cost of the wastewater treatment [11]. Moreover, a recent study by Hao et al. [16] proves that the TiO_2 film onto SiC foam exhibits an advantageous photocatalytic performance as compared to TiO_2 nanoparticles.

In the open literature, several publications have analyzed structured catalysts for photocatalytic reactions. The most widely employed substrates are ceramic foams [16–27] and, to a lesser extent, metallic foams [28], ceramic monoliths [29,30], metallic wire meshes [31,32] and ceramic fibers [33–34].

The metallic substrates offer advantages such as light weight, availability in different shapes, ease of handling, and high mechanical strength, among others. Elatmani et al. [28] applied aluminum foam and recycled aluminum swarf machining waste as substrates to be coated with TiO_2 via the sol–gel method. They claimed that these two substrates were able to deliver good absorption of incident flux, in agreement with the results obtained by Plantard et al. [13], who used three types of aluminum foams. However, neither study offers a physicochemical and textural characterization of the TiO_2 films so obtained nor a description of their chemical and mechanical stabilities. Metallic substrates usually need a passivation process to avoid further metallic segregation and to generate enough surface roughness that improves the anchorage of the catalytic coating [35]. Relatively inexpensive stainless steel foams turn out to be interesting as metallic substrates due to the oxide layer formation after submitting at high temperatures. Among them, AISI 314 foams are characterized by a chromium-rich oxide layer after being treated at 900 °C for 10 h [35].

The whole process of immobilizing titania films onto substrate walls can induce modifications on the TiO_2 structure and, as consequence, on its photocatalytic performance. In this vein, the cation migration from the substrate core to the TiO_2 film during the coating manufacture should be controlled. Cations such as Cr^{3+} and Fe^{3+} from stainless steel, Na^{+} and Si^{4+} from glass [14] can modify the electron–hole recombination sites of TiO_2.

Besides, the coating thickness and its adherence play an important role associated with the film mechanical stability and the reactant accessibility to the active sites. Furthermore, there is a decrease in the catalytic surface area available for reaction depending on the substrate geometry. Foams, the substrate used in this work, have a characteristic open three-dimensional structure. This type of geometry minimizes the reduction in surface area and improves flow turbulence and light permeability, thus promoting a higher contact between the catalyst coating and the wastewater [19].

Different methods for the immobilization of TiO_2 on rigid substrates have been investigated such as electrophoretic and spray coating, electrochemical anodization [36], dip-coating and washcoating [37], among others. The latter procedure employs a TiO_2 suspension that can be made from sol–gel techniques [16,22,24], nano-particles [21,25] or micro-particles [17,20,26].

In this work, metallic foams of 50 pores per linear inch –ppi– (Porvair®) were employed as substrates in order to increase the geometric area on which the catalytic coatings were produced via washcoating. This method is characterized by its simplicity [38], using a TiO_2 microparticles suspension (Degussa P25) with additives to improve its adhesion and its chemical stability. The main objective of this contribution was to generate a homogeneous TiO_2 film onto the metallic foam walls with high adherence, free of cations from the foam core and maintaining the crystalline composition of the commercial TiO_2 (P25).

The structured catalysts so obtained were evaluated in the photocatalytic degradation of nonylphenol ethoxylate with 4 degrees of ethoxylation (NP_4EO). This compound is a surfactant employed in the electroplating industry as alkaline degreaser and is considered an endocrine disruptor. In order to compare the results obtained, the photocatalytic activity of the commercial meshes (TiO_2–Ti mesh, De Nora® of Brazil) was also assessed. TiO_2–Ti mesh De Nora of Brazil was used as a reference catalyst since it is already a commercial product sold to be used in water treatment plants. Nevertheless, this mesh is commercially used as a DSA® electrode on electrochemical processes. Its use in photocatalytic processes is still a matter of research [39–41].

During the different steps of the synthesis process, the structured catalysts (foam + coating) were characterized by various techniques such as Scanning Electron Microscopy (SEM), Laser Raman Spectroscopy and X-ray Diffraction (XRD).

2. Experimental

2.1. Foam pretreatment

The substrates used were stainless steel AISI 314 foams (Porvair® Advanced Materials, 50 pores per linear inch –ppi–). They were cut in pieces with dimensions of 35 mm × 25 mm × 5 mm. The organic impurities of these foam pieces were removed by washing with acetone in an ultrasound bath for 30 min. After that, the foams were dried in an oven at 120 °C for 120 min. The inorganic impurities were then removed by washing with deionized water in an ultrasound bath for 30 min with a drying process at 120 °C for 120 min.

After cleaning, the foams were weighed and calcined at 900 °C for 600 min in a muffle furnace (static air), using a heating rate of 5 °C min^{-1}, and then cooled down to room temperature. After calcination, the foams were weighed again and the weight gain percentage was determined [35].

2.2. TiO_2 immobilization onto the foam surface

The procedure employed a TiO_2 dipping suspension, which contained 20.2 g of deionized water, 0.6 g of polyvinyl alcohol (PVA, Sigma Aldrich), 6.8 g of colloidal suspension which contained nanoparticles of zirconium oxide (Nyacol, 20%wt. of solids amount, acetate stabilized, dp = 100 nm) [35] and 3.2 g of AEROXIDE TiO_2 P-25 powder (Evonik; 50 m^2 g^{-1}, 80% anatase: 20% rutile, mean particle diameter 21 nm). Nanoparticles of ZrO_2 were incorporated to the suspension to assist with the adherence of TiO_2 particles onto the substrate walls and their cohesion. On the other hand, the addition of PVA was performed to improve the suspension rheological properties.

The TiO_2 immobilization was done by immersion of the pretreated foam into the dipping suspension placed in an ultrasound bath during 1 min, and then drying at 120 °C for 60 min. These two steps (I) were repeated twice. After that, a calcination step (C) was carried out at 500 °C for 60 min with a heating rate of 5 °C min^{-1} [42]. Next, the titania-coated foam (TiO_2-foam) was submitted to an ultrasound treatment (U) in deionized water for 30 min. In brief, the process cycle consisted of the following steps: I → I → C → U and this cycle was repeated twice.

2.3. Characterization of the pretreated foam and TiO_2-foam

The X-ray diffraction patterns (XRD) were recorded using Cu Kα radiation over a 20–80° range at a scan rate of 2° min^{-1}, operating at 30 kV and 40 mA (Shimadzu XD-D1 diffractometer). The software package of the equipment was used for phase identification.

The Laser Raman (LRS) spectra were recorded using a LabRam spectrometer (Horiba-Jobin-Yvon) coupled to an Olympus confocal microscope (a 100 × objective lens was used for simultaneous illumination and collection) and equipped with a CCD detector cooled about −70 °C using the Peltier effect. The excitation wavelength was in all cases 532.13 nm (Spectra Physics diode pump solid state laser). The laser power was established at 30 mW.

The morphology of the pretreated foam and TiO_2-foam were analyzed by Scanning Electron Microscopy (SEM) with a JEOL JSM-35C microscope operating at 20 kV, equipped with EDX energy-dispersive system. The sample coating procedures were performed using a combined gold/carbon deposition of metals SPI supplies 12157-AX under argon atmosphere.

2.4. Heterogeneous photocatalysis system

The photocatalytic activity of the TiO_2-foam was analyzed using the photocatalytic degradation of nonylphenol ethoxylate surfactant (NP_4EO). The photoreactor scheme employed is shown in Fig. 1. Besides, the photocatalytic activity of the commercial TiO_2–Ti mesh (rhomboid open area: 9 × 2 mm, De Nora of Brazil®) was also assessed using the same reaction conditions in order to compare both photocatalytic performances. The TiO_2 film in this commercial TiO_2–Ti mesh was produced by the thermal decomposition of the Ti precursor in an oxygen atmosphere.

The ULTRANEX® NP40 (99.5%) commercial surfactant was used as a source of NP_4EO. The initial solution was prepared by diluting the commercial surfactant in distilled water until a final concentration of 128 μM NP_4EO was achieved. A jacket borosilicate glass reactor with a capacity of 2 L was employed, operated in batch mode and connected to an ultra-thermostatic bath to control the temperature. The 250 W high-pressure commercial mercury vapor lamp, without the glass bulb and inside a quartz tube, was used as a source of UV irradiation [43]. The photocatalysts (TiO_2-foam and commercial TiO_2-Ti) were placed along the outer wall of the quartz bulb with a Teflon support. The catalysts were placed concentrically in the reactor as shown in Fig. 1.

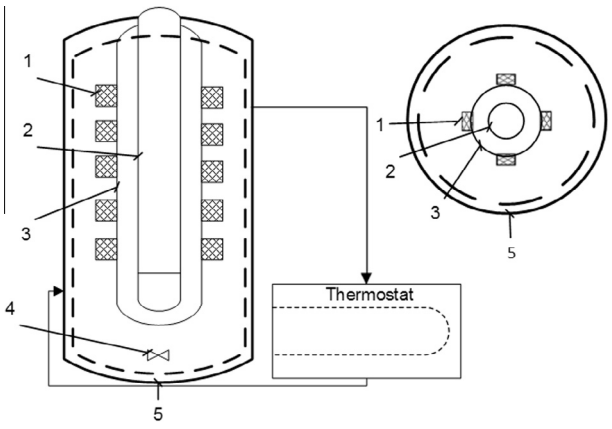

Fig. 1. Scheme of the photocatalytic reactor. (1) TiO_2-foam or TiO_2–Ti. (2) Radiation source. (3) Quartz tube. (4) Stirrer. (5) Glass reservoir.

2.5. Photocatalytic activity measurement

The mineralization was monitored by total organic carbon analysis (TOC-L CPH Shimadzu) during each reaction cycle. The cycle reaction time was 10 h and reused cycles were 10.

The pH of the solution was determined by the potentiometric method using a DM-22 Digimed pH meter.

The measurement of incident irradiation (E, in W m^{-2}) on the catalyst surface when ultrapure water or the initial solution were inside the reactor were determined to the high-pressure commercial mercury vapor lamp (250 W) by an Instrutherm MRUR-203 UV light meter.

The E value (W m^{-2}) can be converted to photon flux using Planck's Eq. (1):

$$E_p = \frac{h \times c}{\lambda} \tag{1}$$

where h is Planck's constant (6.626×10^{-34} J s), c is the speed of light (2.998×10^{8} m s^{-1}) and λ is the wavelength (nm) based on the photometric data of the 250 W lamp used in this work, λ = 365 nm. Taking these values into account, $E_p = 5.44 \times 10^{-19}$ J.

The number of photons (N_p) can then be calculated by (2):

$$N_p = \frac{E}{E_p}\left(\frac{1}{m^2\,s}\right) \tag{2}$$

With the N_p value, the photon flux (E_{qf}) will be determined by (3):

$$E_{qf} = \frac{N_p}{N_A}\left(\frac{mol}{m^2\,s}\right) \tag{3}$$

where N_A is the Avogadro number (6.02×10^{23} mol^{-1}).

The reaction kinetic constant (k') was calculated based on the TOC results, assuming that in most cases the photocatalytic degradation kinetics of general pollutants in aqueous solution is described by a Langmuir–Hinshelwood model (4) [44–46].

$$-k' \times t = \ln\left(\frac{c}{c_0}\right) \tag{4}$$

where, t is the exposure time; k' is the kinetic constant; C_0 is the TOC of initial effluent and C is the TOC at any time during the photocatalytic reaction.

Another significant parameter to evaluate the photocatalysis is the overall quantum yield ($\Phi_{overall}$), defined as the number of molecules undergoing an event (conversion of reactants or formation of products) relative to the number of photons absorbed by the photocatalyst. With the photon flux that arrives at the catalyst surface, the overall quantum yield ($\Phi_{overall}$) of a photocatalysis reaction was calculated, assuming that all photons are absorbed by the semiconductor and that actual light-scattering losses out of the reaction cell are negligible, according to Eq. (5) [47]:

$$\Phi_{overall} = \frac{k'}{E_{qf}} \quad (5)$$

2.6. Adherence tests of TiO_2 coating onto a metallic foam substrate

The adherence of TiO_2 coatings onto the foam supports (AISI 314 50ppi) was evaluated examining the mass loss of TiO_2 coatings during ten cycles of reaction tests. The mass change and photocatalytic activity of the TiO_2-foam were recorded after each test cycle.

3. Results and discussion

3.1. Characterization of the calcined foam

The original foam (Fig. 2(a)), made of austenitic stainless steel, has 50 ppi with polyhedral cells interconnected through hollow struts and windows. Besides, the cell surface morphology is smooth, which hinders the correct immobilization of the TiO_2 particles.

Bortolozzi et al. [35] were the first authors to report that in order to preserve the open polyhedral cell structure and the mechanical properties and, at the same time, generate an oxide layer on the cell surface, the optimal calcination conditions are 900 °C and 10 h (Fig. 2(b)).

This layer not only induces the passivation of the metallic surface but also provides enough roughness to favor a correct anchorage of titania particles. The oxide layer thus formed contains chromium (III) oxide (Cr_2O_3, JCPDS 38-1479), manganese-chromium spinel ($Mn_{1+x}Cr_{1-x}O_{4-x}$, JCPDS 33-892), iron–chromium spinel ($FeCr_2O_4$, JCPDS 34-140) and iron (III) oxide (Fe_2O_3, JCPDS 33-664) (Fig. 3). Since austenitic stainless steel diffractions at 2θ: 43.6°, 50.8°, 74.7° (JCPDS 33-397) [48] are identified in the X-ray diffraction pattern of the treated foam (Fig. 3), the metallic core of the foam is preserved.

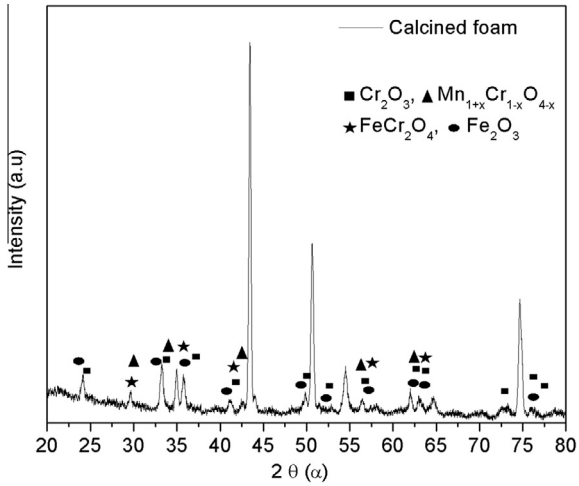

Fig. 3. Foam crystalline phases after being calcined at 900 °C for 600 min.

3.2. Characterization of TiO_2 films onto the foam walls

The titania immobilization was performed in ten pretreated foam pieces. The average mass gain percentage in each cycle step is represented in Fig. 4. The bars indicate the standard deviations (SD). Even though all SDs were high, the mass evolutions of each piece were quite similar, suggesting that the deviation in each step was associated with the different masses of each original foam piece.

During the calcination step (C), the water and polyvinyl alcohol present in the coatings, were removed with the consequent mass loss. In addition, the weakly adhered TiO_2 particles were removed during the ultrasonic bath step. After the complete first cycle (I + I + C + U), the average mass gain was 12% and after the second one, this value rose up to 20%.

The XRD was employed to characterize the crystalline phases of the TiO_2 film, immobilized on the foam walls (TiO_2-foam). Fig. 5 presents the X-ray diffractogram of the TiO_2-foam in comparison with that of the powdered TiO_2 Degussa P25. The peaks of crystalline anatase and rutile are clearly identified in both diffractograms, confirming that the titania film obtained onto this substrate (TiO_2-foam) maintained the same phases as the original powder. This is a significant observation because the excellent photoactivity results are mainly linked to the crystalline

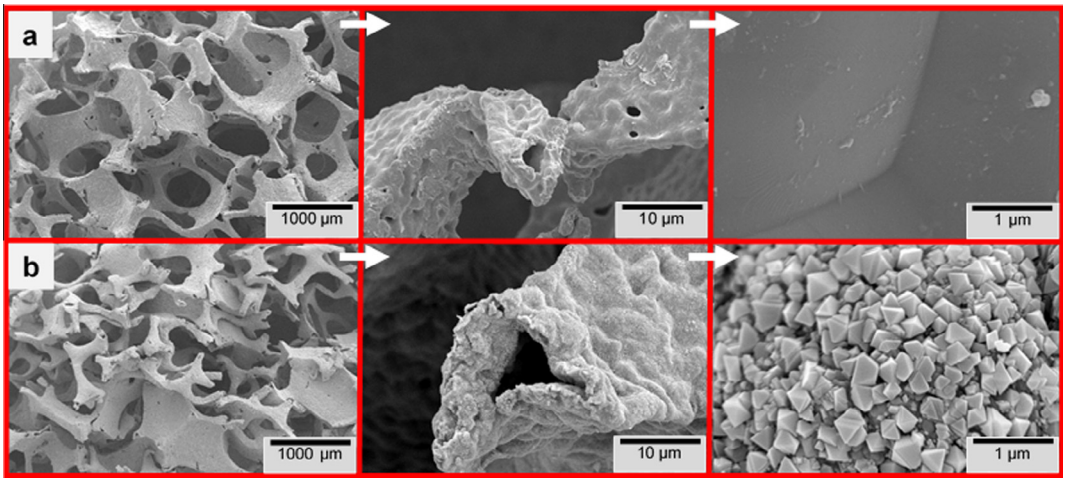

Fig. 2. Wall morphology of the original foam (a) and the calcined foam at 900 °C during 600 min (b).

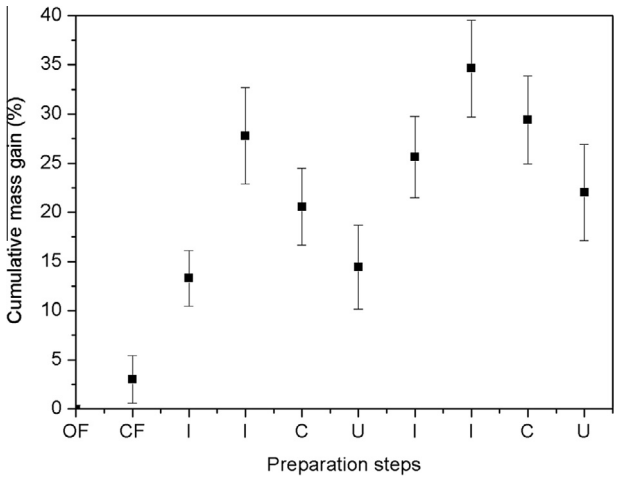

Fig. 4. Cumulative mass gain in relation to the cycle steps (OF: original foam. CF: calcined foam. I: immersion in TiO_2 suspension. C: calcination. U: ultrasonic treatment).

composition of anatase and rutile, found in the commercial Degussa P25 (70/80:30/20) [5,6,49]. Moreover, the thickness of TiO_2 coatings so obtained are high, around 1–3 μm and because of that the characteristic reflections of austenitic stainless steel (Fig. 3, 2θ: 43.6, 50.8 and 74.7° (JCPDS 33-397)) are absent in the TiO_2-foam diffractogram (Fig. 5).

Anatase is generally regarded as the most photochemically active phase of titania, presumably due to the combined effect of lower rates of recombination and higher surface adsorptive capacity [50,51]. This phase of TiO_2 has a band gap of 3.2 eV, corresponding to a UV wavelength of 385 nm, showing an adsorptive affinity for organic compounds higher than the one of rutile [50]. In contrast, rutile has a smaller band gap (3.0 eV) with wavelengths that extend into the visible at 410 nm. Nevertheless, as mentioned above, the coexistence of both phases, anatase and rutile, with appropriate distribution generates a synergetic behavior, improving the photocatalytic performance by inhibiting the recombination of electron–hole pairs [5,6]. According to C. Thurnauer and coworkers, TiO_2 P25 is formed by nanoclusters containing atypically small rutile crystallites interwoven with anatase crystallites [5].

Fig. 6 presents the Raman spectra of the samples: Degussa P25 in powder form (Fig. 6(a)) and TiO_2-foam (Fig. 6(b)). According to factor group analysis, anatase shows six Raman active modes ($A_{1g} + 2B_{1g} + 3_{Eg}$). In a Raman spectrum of an anatase single crystal, the six allowed modes appear at 144 (E_g), 197 (E_g), 399 (B_{1g}), 513 (A_{1g}), 519 (B_{1g}) and 639 cm^{-1} (E_g). In contrast, the rutile phase has only four Raman active modes: B_{1g}, E_g, A_{1g}, and B_{2g} at 143, 447, 612, and 826 cm^{-1}, respectively [52,53]. The characteristic Raman active phonons of anatase were observed in the LR spectra of powder titania and TiO_2-foam (Fig. 6(a) and (b)) with a contribution of two shoulders around 440 and 610 cm^{-1}, attributed to the rutile phase (pointed out with arrows). This fact confirms that the immobilization process produced a titania film which maintains the phases of interest and also corroborates the above XRD results.

The SEM micrographs of the films obtained by the washcoating method (TiO_2-foam) show a homogeneous and well-spread titania layer, without blocking the foam pores (Fig. 7). However, in some sectors, the coating presents some cracks with average sizes of 0.3–0.5 μm. The average thickness of this layer, estimated by cross-section SEM micrographs, is around 1–3 μm. These film fractures may be due to either the coating contraction and/or stress during the drying process or it may occur during the annealing (calcination) due to different thermal expansion coefficients of the TiO_2 layer and the metallic substrate (AISI 314, 50 ppi).

The durability and mutual adherence between the substrate and the coating are important features which must be considered for structured catalysts, especially when used in water and wastewater treatment applications.

Thus, the adherence of TiO_2 coatings onto the metallic foams was evaluated by examining the mass loss of TiO_2 coatings during

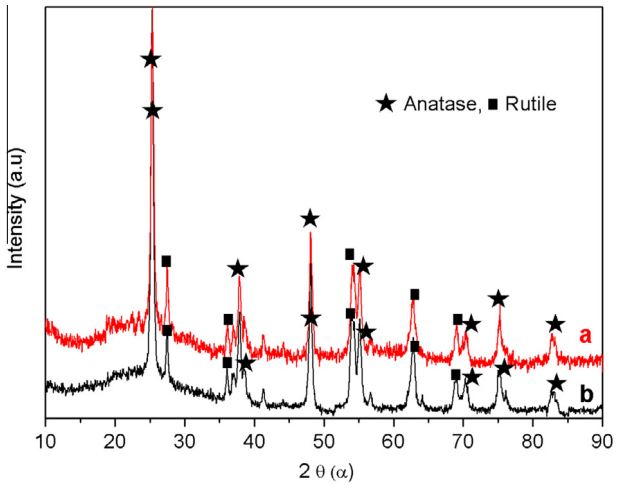

Fig. 5. XRD comparison of Degussa P25 (a) and TiO_2-foam (b).

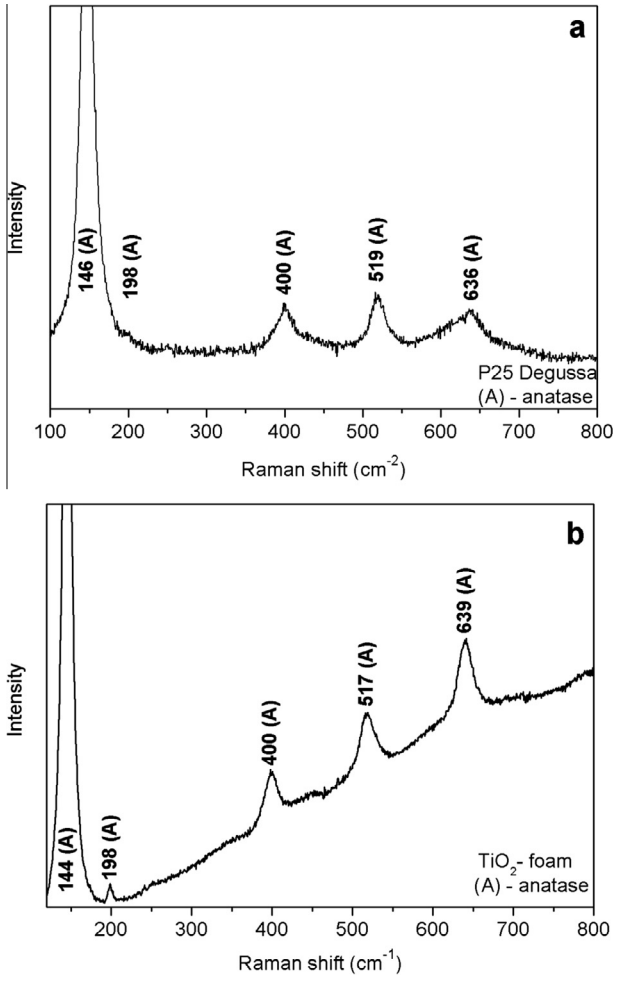

Fig. 6. Raman spectra of: Degussa P25 (a) and TiO_2-foam (b). Arrows: signals attributed to the rutile phase.

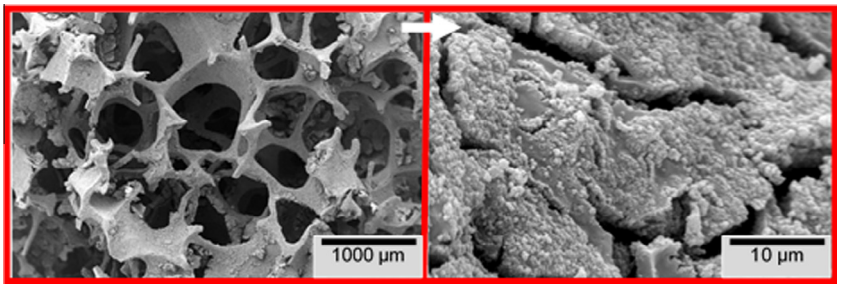

Fig. 7. SEM micrographs of the TiO_2 film onto the metallic foam.

ten cycles of photocatalytic degradation of the NP_4EO surfactant. The mass change of the TiO_2-foam and the commercial catalyst (TiO_2–Ti mesh) are shown in Fig. 8. The TiO_2-foam shows a small mass gain (99.9 ± 20.4 mg) after 10 cycles of photocatalysis tests, the average mass gain being around 6.8% in weight. This mass increase can be attributed to deposits of byproducts related to NP_4EO degradation on the catalyst surface. These byproducts can polymerize on the catalyst surface thereby increasing their mass. Then, three consecutive washing solutions were applied to clean the used TiO_2-foam photocatalysts composed of: the first one, alcoholic KOH 20%, the second one, distilled and deionized water and the last one, a solution of HCl 0.001 M. Fig. 8 shows that, after the TiO_2-foam cleaning step, the mass presents very similar values compared to the initial ones. This evidence demonstrates that there is no significant mass loss after use in reaction and with the subsequent cleaning operation, thus confirming that the TiO_2 coating layer has been firmly adhered to the AISI 314 foam supports. On the other hand, the commercial catalyst did not show any mass increase (Fig. 8).

3.3. Photocatalytic activity evaluation

In order to prove the photocatalytic activity of the catalysts, one direct photolysis assay of the initial solution using a 250 W lamp was carried out.

Fig. 9 shows the comparative results of the direct photolysis and of the photocatalytic degradation of the emerging contaminant (NP_4EO) using both catalysts, the TiO_2-foam and the commercial TiO_2–Ti.

It can be seen that by direct photolysis of the initial solution, the mineralization of the NP_4EO pollutant is much smaller than the one achieved when the catalyst was added in the reaction. This effect of increasing the mineralization of NP_4EO, with a consequent increase in reaction speed in heterogeneous photocatalysis compared to the direct photolysis process was also shown in previous studies of da Silva et al. [54]. In these studies, da Silva et al. [54] demonstrated that direct photolysis degrades the NP_4EO but does not lead to mineralization. On the other hand, when the catalyst was added the hydroxyl radicals were generated, leading to the mineralization of NP_4EO.

Considering the photocatalysis experiment, in the treatment time of 4 h the mineralization achieves 23% and by increasing the total treatment time to 6 h and 8 h, there is a large increase in mineralization of NP_4EO (56% and 76%, respectively). The mineralization at the final treatment time of 10 h was 91% for both catalysts. Several studies [55–59] indicate that NP_nEO has three units that can be attacked by $HO^{\cdot}$, the chain of ethene oxide, the alkyl chain and the aromatic ring. Moreover, the attack by $HO^{\cdot}$ of different portions leads to different degradation products and different kinetic rates.

Indeed, it can be inferred that the small TOC reduction in the first 4 h of treatment may be linked to the surfactant concentration and consequent micelle formation (Fig. 10(b)). The ethoxylated chains, which are more hydrophilic, should be placed outside this micelle whereas the alkyl chain together with the aromatic ring, which are more hydrophobic, should be placed inside the micelle (Fig. 10(a)). Therefore, the hydrophilic portion, adsorbed at the catalyst surface, is primarily attacked by the hydroxyl radical ($HO^{\cdot}$) forming reaction byproducts (Eq. (6)) [55].

$$HO^{\cdot} + NP_4EO \xrightarrow{k_1} \text{by products (open rings products)} \quad (6)$$

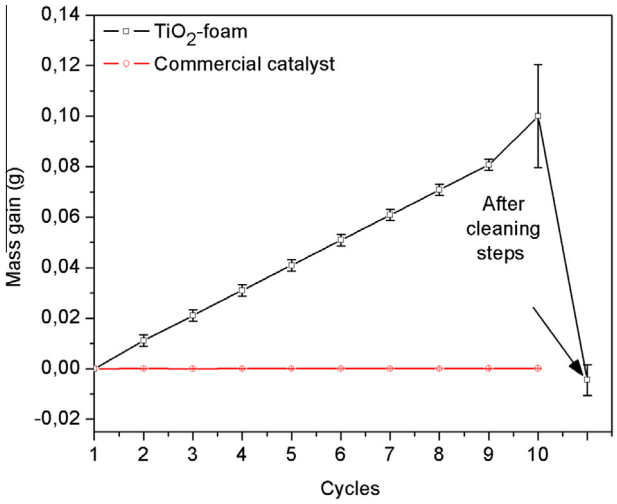

Fig. 8. Mass changes of the TiO_2-foam in ten cycles of reusing.

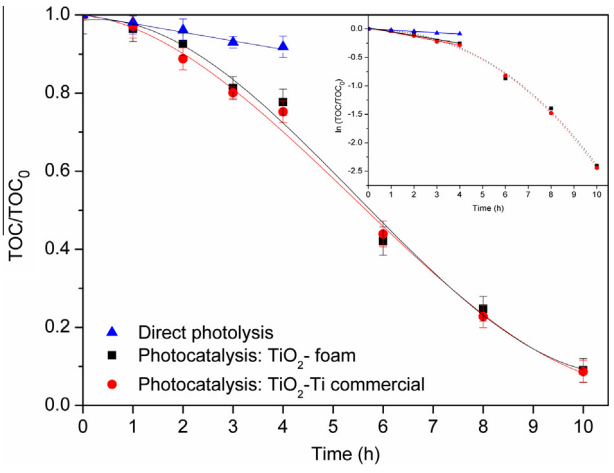

Fig. 9. TOC reduction for the two structured catalysts, TiO_2-foam and TiO_2-Ti mesh (commercial catalyst) and the direct photolysis using a 250 W lamp at different reaction times.

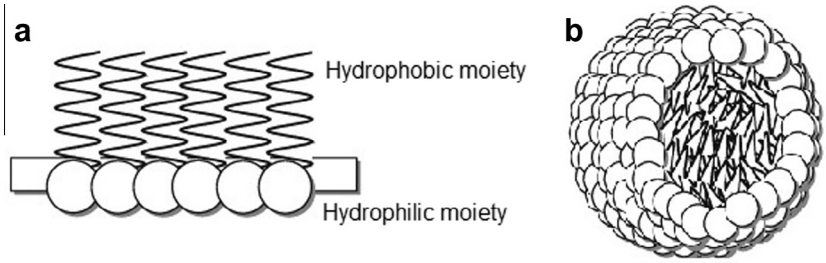

Fig. 10. Surfactant molecules (a) and its micellar arrangement (b).

Table 1
Results of pH measurement.

Solutions	Treatment time (h)	pH
Initial solution	0	5.2 ± 0.3
Treated by direct photolysis	4	4.3 ± 0.5
Treated by photocatalysis: TiO_2-foam	4	4.5 ± 0.4
Treated by photocatalysis: TiO_2–Ti commercial	4	4.6 ± 0.3

As a result, the inserted graph in Fig. 9 shows that in the first four hours of treatment, the reaction presents a first-order kinetics ($\ln [TOC/TOC_0]$ is linear) exhibiting a k_1 value of 0.001 min^{-1} and 0.0011 min^{-1}, respectively, to both catalysts, the TiO_2-foam and the commercial TiO_2–Ti. Then, after 4 h of treatment, there is an increased exposure of alkyl chain and aromatic ring, leading to a significant increase in the complete mineralization of this surfactant (Eq. (7)).

$$HO^{\cdot} + \text{by products (open rings products)} \times \xrightarrow{k_2} (\text{mineralization products}) \quad (7)$$

After the final treatment time (10 h) the reaction kinetic constants for the TiO_2-foam and TiO_2–Ti mesh were 0.004013 min^{-1} and 0.004084 min^{-1}, respectively, showing pseudo first-order kinetics (inserted graph in Fig. 9). It is remarkable that the kinetic constant, k_2 is higher than k_1. This fact may be linked to the open rings degradation products and the decrease in the NP_4EO concentration in the solution. Since the surfactant is not in micellar form (Fig. 10(b)), it is more easily degraded than the pattern product (NP_4EO).

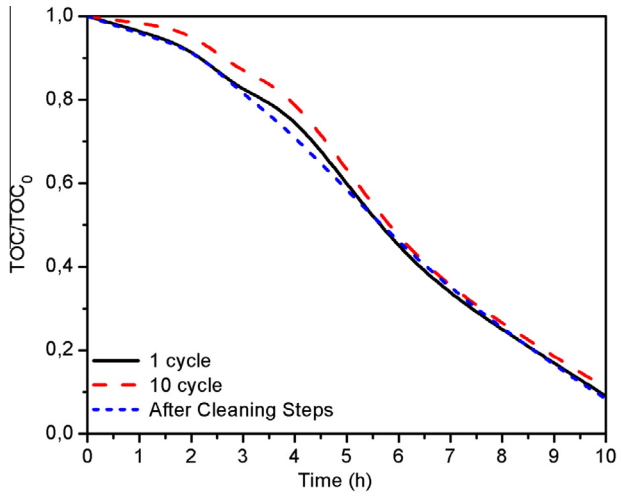

Fig. 11. TOC reduction for the TiO_2-foam in ten cycles of reusing and one cycle after the cleanup procedure.

The presence of organic acids would imply a decrease of the solution pH. Table 1 shows that, independently of the treatment and of the catalyst used, the final solution pH is lower than the initial one. According to Socha et al. [60], the reaction rate does not depend on pH in the range from 3.5 to 10.

For the 250 W lamp, the photon flux that arrives at the catalyst surface when the reactor is full with ultrapure water is 1.78×10^{-5} mol m^{-2} s^{-1}. On the other hand, when the reactor is full with the initial NP_4EO solution, the photon flux that arrives at the catalyst is 1.41×10^{-5} mol m^{-2} s^{-1}. This means that the initial solution absorbs some radiation, i.e. 3.66×10^{-6} photons are absorbed, meaning that it is possible to achieve some degradation by direct photolysis. Moreover, 1.41×10^{-5} mol m^{-2} s^{-1} arrives at the catalyst surface favoring the heterogeneous photocatalysis. These results corroborate the results of TOC removal in Fig. 9, which shows that although direct photolysis degrades the NP_4EO, the higher mineralization was obtained after the heterogeneous photocatalysis process.

Furthermore, the $\Phi_{overall}$ result for both catalysts is about 0.28 or 28%. It is observed that there were no significant differences in photocatalytic activity between the prepared supported catalyst (TiO_2-foam) and the commercial one (TiO_2–Ti).

After ten cycles reusing the TiO_2-foam, there was a slight reduction in photocatalytic activity (Fig. 11). This reduction of photocatalytic activity may have occurred due to the mass increase shown in Fig. 8. The deposit of degradation byproducts could decrease the active surface of the catalyst. Nevertheless, it must be noted that after the cleaning step, i.e. cycle number 11, the photocatalytic activity increases again. Therefore, the organic film which reduced the photocatalytic activity was completely removed. In the TiO_2–Ti mesh commercial catalyst, the loss of catalytic activity was not observed. These results are in good agreement with the ones presented in Fig. 8, in which no mass gain was observed.

The geometric characteristics of the foams and their assemblage in the photo-reactor configuration may have been the reason for the polymerization of the degradation byproducts on the TiO_2-foam catalyst surface. This could be related to the fact that this structured catalyst has relatively smaller pore sizes (average diameter: 0.5 mm) compared with those of the commercial TiO_2–Ti mesh (rhomboid open area: 9 × 2 mm). Besides, the TiO_2-foam pieces were adhered to the quartz surface, bringing some difficulties to the solution flow between the quartz walls and the TiO_2-foam system. This difficulty was not present when the commercial TiO_2–Ti mesh was used as photocatalyst, since this mesh was placed concentrically outside the quartz walls. In consequence, the deposit of polymerized degradation byproducts on the catalyst surface could be easily avoided by (i) the modification of TiO_2-foam piece configuration in the way of improving the flow between the TiO_2-foam catalyst and quartz bulb and (ii) using foams with larger pore sizes. These two items will be the object of further research.

In addition, modifications in the composition of "washcoating" slurry and/or in the calcination procedure could be introduced in order to minimize the generation of cracks spread over the

coatings. Improvements of the film smoothness could also be achieved [61,62].

4. Conclusions

In this work, it was demonstrated that a fast and easy washcoating method allowed the immobilization of a commercially available powder TiO_2 onto a relatively inexpensive metallic substrate. The TiO_2 layer was uniformly distributed, having a high adherence to the metallic foam walls, which were previously submitted to a passivation treatment (900 °C for 10 h). This pre-treatment hinders further cations migration from the foam core to the titania film and favors the subsequent film anchorage.

The XRD and Raman results showed the maintenance of the anatase phase in higher proportion than the rutile phase in the TiO_2-foam, preserving the original properties of the TiO_2 powder since they are important for its photoactivity and stability.

The results in mineralization of the surfactant NP_4EO using TiO_2-foam are very similar compared to a much more expensive commercial catalyst (TiO_2-Ti mesh), with a metal substrate made of titanium.

With a fast washing stage, first in a basic solution, then in a water and acid solution, the structured catalyst employed totally recovered its photoactivity, after a small deactivation occurred during the ten catalytic tests.

Based on these results, the use of immobilized TiO_2 on low cost substrates emerges as a viable alternative for heterogeneous photocatalysis for the water/wastewater treatment. With this method, the catalyst recovery steps are avoided, thus reducing the overall cost of the process.

Acknowledgment

The authors would like to acknowledge the financial support of CNPq, FAPERGS, FINEP and CAPES project PPCP 005/2011 and CAPG-BA 73/14 from Brazil and of PPCP-MERCOSUR, CAPG-BA 73/14, ANPCyT, CONICET, and UNL from Argentina.

References

[1] S. Malato, P. Fernández-Ibáñez, M.I. Maldonado, J. Blanco, W. Gernjak, Decontamination and disinfection of water by solar photocatalysis: recent overview and trends, Catal. Today 147 (2009) 1–59.
[2] G. Plantard, T. Janin, V. Goetz, S. Brosillon, Review: solar photocatalysis treatment of phytosanitary refuses: efficiency of industrial photocatalysts, Appl. Catal. B 115–116 (2012) 38–44.
[3] H. Selcuk, M. Bekbolet, Photocatalytic and photoelectrocatalytic humic acid removal and selectivity of TiO_2 coated photoanode, Chemosphere 73 (2008) 854–858.
[4] Z. Wang, C. Chen, F. Wu, B. Zou, M. Zhao, J. Wang, C. Feng, Photodegradation of rhodamine B under visible light by bimetal codoped TiO_2 nanocrystals, J. Hazard. Mater. 164 (2009) 615–620.
[5] D.C. Hurum, A.G. Agrios, K.A. Gray, T. Rajh, M.C. Thurnauer, Explaining the enhanced photocatalytic activity of degussa P25 mixed-Phase TiO_2 using EPR, J. Phys. Chem. B 107 (2003) 4545–4549.
[6] S. Ahmed, M.G. Rasul, W.N. Martens, R. Brown, M.A. Hashib, Heterogeneous photocatalytic degradation of phenols in wastewater: a review on current status and developments, Desalination 261 (2010) 3–18.
[7] S.P. Patkowska, B. Czech, J. Ryczkowski, J. Patkowski, Removal of recalcitrant pollutants from wastewater, Appl. Surf. Sci. 256 (2010) 5434–5438.
[8] R. Vinu, G. Madras, Environmental remediation by photocatalysis, J. Indian Inst. Sci. 90 (2010). 289-230.
[9] M.R. Hoffmann, S.T. Martin, W. Choi, D.W. Bahnemann, Environmental applications of semiconductor photocatalysis, Chem. Rev. 95 (1995) 69–96.
[10] S. Chen, Y. Liu, Study on the photocatalytic degradation of glyphosate by TiO_2 photocatalyst, Chemosphere 67 (2007) 1010–1017.
[11] A. Mills, R.H. Davies, D. Worsley, Water purification by semiconductor photocatalysis, Chem. Soc. Rev. 22 (1993) 417–425.
[12] G. Plantard, V. Goetz, F. Correia, J.P. Cambon, Importance of a medium's structure on photocatalysis: using TiO_2 coated foams, Sol. Energy Mater. Sol. Cells 95 (2011) 2437–2442.
[13] G. Plantard, V. Goetz, D. Sacco, TiO_2-coated foams as a medium for solar catalysis, Mater. Res. Bull. 46 (2011) 231–234.
[14] J.-M. Herrmann, H. Tahiri, C. Guillard, P. Pichat, Photocatalytic degradation of aqueous hydroxy-butandioic acid (malic acid) in contact with powdered and supported titania in water, Catal. Today 54 (1999) 131–141.
[15] A. Fernández, G. Lassaletta, V.M. Jiménez, A. Justo, A.R. González-Elipe, J.M. Herrmann, H. Tahiri, Y. Ait-Ichou, Preparation and characterization of TiO_2 photocatalysts supported on various rigid supports (glass, quartz and stainless steel). Comparative studies of photocatalytic activity in water purification, Appl. Catal. B 7 (1995) 49–63.
[16] D. Hao, Z. Yang, C. Jiang, J. Zhang, Synergistic photocatalytic effect of TiO_2 coatings and p-type semiconductive SiC foam supports for degradation of organic contaminant, Appl. Catal. B 144 (2014) 196–202.
[17] S. Qiu, S. Xu, F. Ma, J. Yang, The photocatalytic efficiency of the metal doped TiO_2 with ceramic foam as catalyst carriers, Powder Technol. 210 (2011) 83–86.
[18] W.A. Zeltner, C.G.J. Hill, M.A. Anderson, Supported titania for photodegradation, Chem. Tech. 23 (1993) 21–29.
[19] I.J. Ochuma, O.O. Osibo, R.P. Fishwick, S. Pollington, A. Wagland, J. Wood, Three-phase photocatalysis using suspended titania and titania supported on a reticulated foam monolith for water purification J.M. Winterbottom, Catal. Today 128 (2007) 100–107.
[20] G. Plesch, M. Gorbár, U.F. Vogt, K. Jesenák, M. Vargová, Mater. Reticulated macroporous ceramic foam supported TiO_2 for photocatalytic applications, Mater. Lett. 63 (2009) 461–463.
[21] A.N. Kouamé, R. Masson, D. Robert, N. Keller, V. Keller, β-SiC foams as a promising structured photocatalytic support for water and air detoxification, Catal. Today 209 (2013) 13–20.
[22] N.A. Kouamé, D. Robert, V. Keller, N. Keller, C. Pham, P. Nguyen, Preliminary study of the use of β-SiC foam as a photocatalytic support for water treatment, Catal. Today 161 (2011) 3–7.
[23] N. Doss, P. Bernhardt, T. Romero, R. Masson, V. Keller, N. Keller, Photocatalytic degradation of butanone (methylethylketone) in a small-size TiO_2/β-SiC alveolar foam LED reactor, Appl. Catal. B 154–155 (2014) 301–308.
[24] N.A. Kouamé, D. Robert, V. Keller, N. Keller, C. Pham, P. Nguyen, TiO_2/β-SiC foam-structured photoreactor for continuous wastewater treatment, Environ. Sci. Pollut. Res. Int. 19 (2012) 3727–3734.
[25] Y. Yao, T. Ochiai, H. Ishiguro, R. Nakano, Y. Kubota, Antibacterial performance of a novel photocatalytic-coated cordierite foam for use in air cleaners, Appl. Catal. B 106 (2011) 592–599.
[26] S. Hajiesmaili, S. Josset, D. Bégin, C. Pham-Huu, N. Keller, V. Keller, 3D solid carbon foam-based photocatalytic materials for vapor phase flow-through structured photoreactors, Appl. Catal. A 382 (2010) 122–130.
[27] M. Vargová, G. Plesch, U.F. Vogt, M. Zahoran, M. Gorbár, K. Jesenák, TiO_2 thick films supported on reticulated macroporous Al_2O_3 foams and their photoactivity in phenol mineralization, Appl. Surf. Sci. 257 (2011) 4678–4684.
[28] K. Elatmani, G. Plantard, D. Sacco, I. Aitichou, V. Goetz, Innovative photocatalytic media optimized for solar-powered remediation: application to pyrimethanil treatment, Mater. Sci. Semicond. Process. 16 (2013) 1117–1124.
[29] M.L. Sauer, D.F. Ollis, Acetone oxidation in a photocatalytic monolith reactor, J. Catal. 149 (1994) 81–91.
[30] R.G. Changrani, G.B. Raupp, Two-dimensional heterogeneous model for a reticulated-foam photocatalytic reactor, AIChE J. 46 (2000) 829–842.
[31] Y. Zhao, X. Zhang, J. Zhai, J. He, L. Jiang, Z. Liu, S. Nishimoto, T. Murakami, A. Fujishima, D. Zhu, Enhanced photocatalytic activity of hierarchically micro-/nano-porous TiO_2 films, Appl. Catal. B 83 (2008) 24–29.
[32] T.T. Vu, L. del Río, T. Valdés-Solís, G. Marbán, Stainless steel wire mesh-supported ZnO for the catalytic photodegradation of methylene blue under ultraviolet irradiation, J. Hazard. Mater. 246–247 (2013) 126–134.
[33] T. Yuranova, O. Enea, E. Mielczarski, J. Mielczarski, P. Albers, J. Kiwi, Fenton immobilized photo-assisted catalysis through a Fe/C structured fabric, Appl. Catal. B 49 (2004) 39–50.
[34] S. Kumar, A.G. Fedorov, J.L. Gole, Photodegradation of ethylene using visible light responsive surfaces prepared from titania nanoparticle slurries, Appl. Catal. B 57 (2005) 93–107.
[35] J.P. Bortolozzi, E.D. Banús, V.G. Milt, L.B. Gutierrez, M.A. Ulla, The significance of passivation treatments on AISI 314 foam pieces to be used as substrates for catalytic applications, Appl. Surf. Sci. 257 (2010) 495–502.
[36] J.A. Byrne, B.R. Eggins, N.M.D. Brown, B. McKinney, M. Rouse, Immobilisation of TiO_2 powder for the treatment of polluted water, Appl. Catal. B 17 (1998).
[37] M. Mann, G.E. Shter, G.S. Grader, Effect of sintering on TiO_2-impregnated alumina foams, J. Mater. Sci. 37 (2002) 4049–4055.
[38] A. Montebelli, C.G. Visconti, G. Groppi, E. Tronconi, C. Cristiani, C. Ferreira, S. Kohler, Methods for the catalytic activation of metallic structured substrates, Catal. Sci. Technol. 4 (2014) 2846–2870.
[39] J.M. Aquino, R.C. Rocha-Filho, L.A.M. Ruotolo, N. Bocchi, S.R. Biaggio, Electrochemical degradation of a real textile wastewater using β-PbO_2 and DSA® anodes, Chem. Eng. J. 251 (2014) 138–145.
[40] J.H.B. Rocha, M.M.S. Gomes, N.S. Fernandes, D.R. da Silva, C.A. Martínez-Huitle, Application of electrochemical oxidation as alternative treatment of produced water generated by Brazilian petrochemical industry, Fuel Process. Technol. 96 (2012) 80–87.
[41] E. Tauchert, S. Schneider, J.L. de Morais, P. Peralta-Zamora, Photochemically-assisted electrochemical degradation of landfill leachate, Chemosphere 64 (2006) 1458–1463.
[42] Y. Chen, D.D. Dionysiou, Correlation of structural properties and film thickness to photocatalytic activity of thick TiO_2 films coated on stainless steel, Appl. Catal. B 69 (2006) 24–33.

[43] Philips – HPL High Pressure Mercury, <http://download.p4c.philips.com/l4b/9/928053007495_eu/928053007495_eu_pss_brpbr.pdf>, access in 2015.
[44] M.H. Priya, G. Madras, Kinetics of photocatalytic degradation of phenols with multiple substituent groups, J. Photochem. Photobiol. A 179 (2006) 256–262.
[45] M.F. Fukunaga, J.R. Guimarães, R. Bertazzoli, Kinetics of the oxidation of formaldehyde in a flow electrochemical reactor with TiO_2/RuO_2 anode, Chem. Eng. J. 136 (2008) 236–241.
[46] L. Chen, H.Y. Zhou, Q.Y. Deng, Photolysis of nonylphenol ethoxylates: The determination of the degradation kinetics and the intermediate products, Chemosphere 68 (2007) 354–359.
[47] N. Serpone, Relative photonic efficiencies and quantum yields in heterogeneous photocatalysis, J. Photochem. Photobiol. A 104 (1997) 1–12.
[48] F. Goodwin, S. Guruswamy, K.U. Kainer, C. Kammer, W. Knabl, A. Koethe, G. Leichfried, G. Schlamp, R. Strickler, W. Warlimont, XVIII ed., Springer Handbook of Condensed Matter and Materials Data, 2005.
[49] Y. Bessekhouad, R. Didier, J.V. Weber, Synthesis of photocatalytic TiO_2 nanoparticles: optimization of the preparation conditions, J. Photochem. Photobiol. A 157 (2003) 47–53.
[50] U. Stafford, K.A. Gray, P.V. Kamat, A. Varma, An in situ diffuse reflectance FTIR investigation of photocatalytic degradation of 4-chlorophenol on a TiO_2 powder surface, Chem. Phys. Lett. 205 (1993) 55–61.
[51] G. Riegel, J.R. Bolton, Photocatalytic efficiency variability in TiO_2 particles, J. Phys. Chem. 99 (1995) 4215–4224.
[52] S. Sahoo, A.K. Arora, V. Sridharan, Raman line shapes of optical phonons of different symmetries in anatase TiO_2 nanocrystals, J. Phys. Chem. C 113 (2009) 16927–16933.
[53] F.D. Hardcastle, Raman spectroscopy of titania (TiO_2) nanotubular water-splitting catalysts, J. Arkansas Acad. Sci. 65 (2011) 43–48.
[54] S.W. da Silva, C.R. Klauck, M.A. Siqueira, A.M. Bernardes, Degradation of the commercial surfactant nonylphenol ethoxylate by advanced oxidation processes, J. Hazard. Mater. 282 (2015) 241–248.
[55] S.W. da Silva, G.L. Bordignon, C. Viegas, M.A.S. Rodrigues, A. Arenzon, A.M. Bernardes, Treatment of solutions containing nonylphenol ethoxylate by photoelectrooxidation, Chemosphere 119 (Suppl.) (2015) S101–S108.
[56] E. Pelizzetti, Photocatalytic degradation of nonylphenol ethoxylated surfactants, Environ. Sci. Technol. 23 (1989) 1380–1385.
[57] H. Hidaka, J. Zhao, K. Kitamura, K. Nohara, Photodegradation of surfactants IX: The photocatalysed oxidation of polyoxyethylene alkyl ether homologues at TiO, -water interfaces, J. Photochem. Photobiol. A 64 (1992) 103–113.
[58] H. Hidaka, S. Yamada, S. Suenaga, H. Kubota, Photodegradation of surfactants. V. Photocatalytic degradation of surfactants in the presence of semiconductor particles by solar exposure, J. Photochem. Photobiol. 47 (1989) 102–112.
[59] B.S. Kim, J.M. Philip, R.G. Amiet, M.J. McCormick, Spectroscopic analysis of heterogeneous photocatalysis products of nonylphenol- and primary alcohol ethoxylate nonionic surfactants, Chemosphere 33 (1996) 1921–1940.
[60] A. Socha, E. Chrzescijanska, E. Kusmierek, Photoelectrochemical treatment of 1-amino-8-hydroxynaphthalene-3,6-disulphonic acid at electrode covered with TiO_2/RuO_2, Dyes Pigm. 71 (2006) 10–18.
[61] Y. Chen, D.D. Dionysiou, Bimodal mesoporous TiO_2–P25 composite thick films with high photocatalytic activity and improved structural integrity, Appl. Catal. B 80 (2008) 147–155.
[62] C. Han, M. Pelaez, V. Likodimos, A.G. Kontos, P. Falaras, K. O'Shea, D.D. Dionysiou, Innovative visible light-activated sulfur doped TiO_2 films for water treatment, Appl. Catal. B 107 (2011) 77–87.